Transport through T-shaped quantum wires under potential modulation: Lattice Green's function approach

Yuan Ping Chen, Xiao Hong Yan,* and Yue E. Xie
Institute of Modern Physics and Department of Physics, Xiangtan University, Xiangtan 411105, China
(Received 25 May 2004; revised manuscript received 31 January 2005; published 30 June 2005)

By developing the lattice Green's function approach, we study transport properties of T-shaped quantum wires (TQWR) under potential modulation. It is found that the potential barrier in the vertical arm induces a dip-peak structure in conductance straight through and around the bend. The increase of potential thickness results in the dip-peak couples being more pronounced, while the number of dip-peak couple also increases with the thickness. The dip-peak structures are related to the quasibound states localized at the junction of the TQWR. We numerically analyze the dependence of the quasi-bound state energy on the potential height and width. Different conductance profiles can be selected by the potential modulation on coupled TQWR.

DOI: 10.1103/PhysRevB.71.245335 PACS number(s): 85.35.Be, 73.63.−b

I. INTRODUCTION

Recent developments in semiconductor growth techniques have enabled the fabrication of various nanostructures. As one of interesting structures, T-shaped quantum wires (TQWR) (Ref. 1) can be realized by the epitaxial overgrowth of cleaved edge $GaAs/Al_xGa_{1-x}As$ quantum wells.[2] The structure has attracted much attention because of improved optical properties,[3] such as the excitonic laser emission, the enhancement of excitonic binding energy, and the concentrated oscillator strength. Recently, T-shaped quantum wires (TQWR) were revealed to exhibit interesting transport characteristics.[4–10] Due to the open geometry of TQWR, electrons have possibilities to transmit ballistically across the wire region and show a strong energy dependent transmission as a consequence of quantum interference effect induced by the interplay between the propagating mode of wires. So the junctions in TQWR are found to strongly filter the electrons, changing the distribution of the electrons among the mode of the quantum wire (QWR), while the interference in scattering from two junctions leads to an oscillatory dependence of the transmission on the length between the junctions.[4] By tailoring the widths of the QWRs and/or combining more wires on the scale of the Fermi wavelength, different conductance profiles can be selected.[5] A theoretical study on a periodic array of T-shaped devices[6] shows that deflected arrays exhibit a unique resonance with respect to electrons traveling along the array. The coefficients of the reflection and transmission through the array can peak simultaneously at resonance. Recent experimental photoluminescence spectroscopy analyses[2] and theoretical calculations[7,8] have manifested that there are quantum bound states in TQWR. The existence of these states in such TQWR essentially shows the confinement effect of the mesoscopic geometry in the quantum-mechanical region, and substantially affects the transport properties of the TQWR. It is found that the bound state energies depend strongly on the ratio of the arm widths.[8]

It is well known that the geometry and the potential modulation are important factors to interference of electrons in nanostructures. Various geometries and potential modulation may cause a variety of quantum phenomena, which leads to the manufacture of concept devices with an operation principle entirely based on these quantum phenomena. However, the former studies are only focused on the effect of the geometry of TQWR, without considering potential modulation on transport properties.

In this paper, based on the recursive Green's function (RGF) method,[11,12] we develop a lattice Green's function (LGF) (Refs. 13–15) method to study the transmission through TQWR under potential modulations in vertical arms. The effect of potential height and thickness on transport properties of single and coupled TQWR is discussed. The potential in the vertical arm of TQWR will affect the quasibound states localized at the T junctions, while each quasibound state will induce a dip-peak structure in conductance profiles. Therefore conductance of TQWR can be tailored by choosing appropriate potential height and width.

II. MODEL AND METHOD

Let us consider a single TQWR which is divided into seven parts through dashed lines, as shown in Fig. 1(a), I, V, VII are leads and II, III, IV, VI are middle parts among leads to describe scattering region. Using discreted lattice model, the tight-binding Hamiltonian is given by

$$H=\sum_{i,j}(\varepsilon_{i,j}+P_{i,j})|i,j\rangle\langle i,j|+\sum_{i,j}V_1(|i,j\rangle\langle i,j+1|+\text{H.c.})+\sum_{i,j}V_2(|i+1,j\rangle\langle i,j|+\text{H.c.}),\quad(1)$$

where $\varepsilon_{i,j}$ is the site energy, $P_{i,j}$ is the additional potential at (i,j) site, and V_1 and V_2 are transverse and longitudinal hopping matrix elements between the nearest neighboring sites, respectively. Generally, $\varepsilon_{i,j}=-d*2V$ (d is the number of dimensions) and $V_1=V_2=V=-\hbar^2/2m^*a^2$ in the absence of magnetic modulation ($m^*=0.067m_0$ is effective mass of electron and a is lattice constant). We symbol, respectively, leads I, V, VII with columns 1, n, and row m [see Fig. 1(a)].[11–13]

To describe the transport properties for electrons incident in lead b to be transmitted into lead c, $\mathcal{G}_{cb}$ defined as the

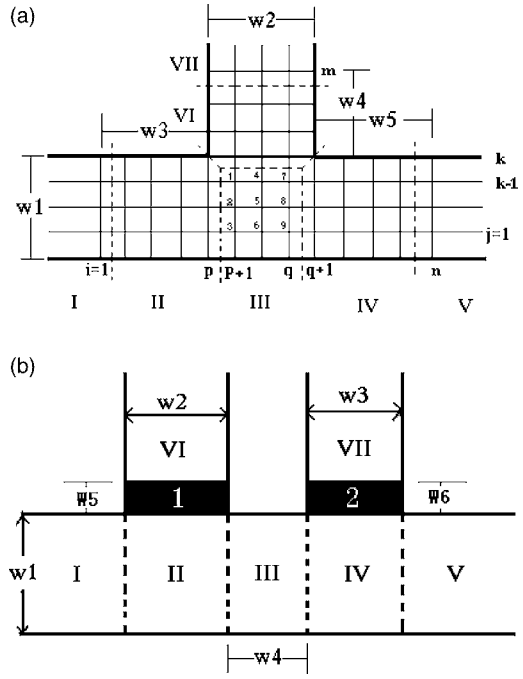

FIG. 1. (a) Schematic view of a single TQWR with $W_1=W_2=10a$. (b) Two coupled TQWR with $W_1=W_2=W_3=W_4=10a$ (a is lattice constant).

Green's function between leads b and c is required first. We take the calculation for the Green's function $\mathcal{G}_{\mathrm{V,I}}$ between parallel leads I and V as an example. Since the TQWR is a multiterminal system, one reformulates the multiterminal problem into an effective two-terminal problem by the "self-energy" term. As shown in Fig. 1(a), row k is viewed as the "surface" of the vertical arm consisting of lead VII and region VI. Using the RGF scheme,[11,12] the Green's function $\mathcal{G}^S$ of the surface is recursively obtained from row m to k. Then the self-energy of the vertical arm can be calculated by $\Sigma = V^2 * \mathcal{G}^S$.[14,15] Taking into account the effect of the vertical arm on region III, the Green's function $\mathcal{G}^R$ of region III is given by[14]

$$\mathcal{G}^R = (E - H_0 - \Sigma)^{-1}, \tag{2}$$

where E is the energy of electrons (in units of $-V$) and H_0 is the Hamiltonian of isolated region III associated with Eq. (1). While the Green's function $\mathcal{G}(q,p+1)$, $\mathcal{G}(p+1,q)$ between column $p+1$ and q, the Green's function $\mathcal{G}(q,q)$ of column q and the Green's function $\mathcal{G}(p+1,p+1)$ of column $p+1$ will be found by extracting elements from $\mathcal{G}^R$, where $\mathcal{G}(r,s)$ denotes the Green's function between column s and column r. Suppose region III has nine sites [see Fig. 1(a)], Eq. (2) can be rewritten as the matrix form

$$\mathcal{G}^R = \begin{pmatrix} g_{1,1} & g_{1,2} & \cdots & g_{1,9} \\ g_{2,1} & g_{2,2} & \cdots & g_{2,9} \\ \cdots & \cdots & \ddots & \cdots \\ g_{9,1} & g_{9,2} & \cdots & g_{9,9} \end{pmatrix}, \tag{3}$$

with $g_{u,v}$ representing the propagation of electrons from point v to u ($u,v=1,2,\ldots,9$). The Green's functions in region III such as $\mathcal{G}(q,p+1)$ and $\mathcal{G}(p+1,p+1)$ can be expressed as

$$\mathcal{G}(q,p+1) = \begin{pmatrix} g_{7,1} & g_{7,2} & g_{7,3} \\ g_{8,1} & g_{8,2} & g_{8,3} \\ g_{9,1} & g_{9,2} & g_{9,3} \end{pmatrix},$$

$$\mathcal{G}(p+1,p+1) = \begin{pmatrix} g_{1,1} & g_{1,2} & g_{1,3} \\ g_{2,1} & g_{2,2} & g_{2,3} \\ g_{3,1} & g_{3,2} & g_{3,3} \end{pmatrix}. \tag{4}$$

As these Green's functions are known, the Green's function $\mathcal{G}(p,1) \rightarrow \mathcal{G}(q,1) \rightarrow \mathcal{G}(n,1)$, i.e., $\mathcal{G}_{\mathrm{V,I}}$ is recursively yielded in turn as Ref. 10.

The Green's function $\mathcal{G}_{\mathrm{V,I}}$ allows us to calculate the transmission coefficient $T_{\mathrm{V,I}}$ in horizontal QWR.[11,12] Conductance straight through the horizontal QWR $G_{\mathrm{V,I}}$ (from leads I to V) is represented by the Landauer-Buttiker formula

$$G_{\mathrm{V,I}} = \frac{2e^2}{h} T_{\mathrm{V,I}}. \tag{5}$$

It should be noted that the method integrates the RGF and ordinary LGF methods to solve the Green's function of intermediate regions in the transverse direction. It reduces the dimension of the Green's function matrix and computing time, which provides a foundation for calculating more complex and large-scale model. The method can also be extended to treat one- and three-dimensional multiterminal system. We calculated the transmission coefficients of one-dimensional multiterminal system as given by Ref. 16. Similar results to those in Ref. 16 were obtained.

To calculate the eigenenergy E of the single TQWR and corresponding wave function Ψ, we write the Hamiltonian of the system as

$$H = H_0 + \Sigma', \tag{6}$$

where H_0 is the total Hamiltonian of regions II, III, IV as well as VI and Σ' is the total self-energies of the three leads. Solving the eigenequation $H\Psi = E\Psi$, one can obtain the eigenenergy and wave function. In general, the eigenvalue is a complex expressed as $E=(E_R,-\gamma)$, in which the real part E_R represents the eigenenergy and the imaginary part γ is associated with the lifetime τ of the eigenstate through $\tau \sim \hbar/2\gamma$.[14] While the liftetime τ is of the order of the reciprocal of the width of the resonance peak ($\hbar/\Delta E$) in the transmission spectrum.[17] So the smaller γ, the longer the lifetime τ, and the narrower the resonance width ΔE in transmission spectrum. In addition, we use the mode-matching method[8,18] to verify the quasibound states and their wave functions.

III. RESULTS AND DISCUSSION

In Figs. 2(a)–2(d), we present the conductance as a function of electron energy for a single TQWR of which a vertical lead VII is connected to a parallel QWR by a potential barrier VI [see Fig. 1(a)]. Solid and dotted lines stand for conductances straight through $G_{\mathrm{V,I}}$ and around the bend $G_{\mathrm{VII,I}}$, respectively. For a perfect TQWR without potential in

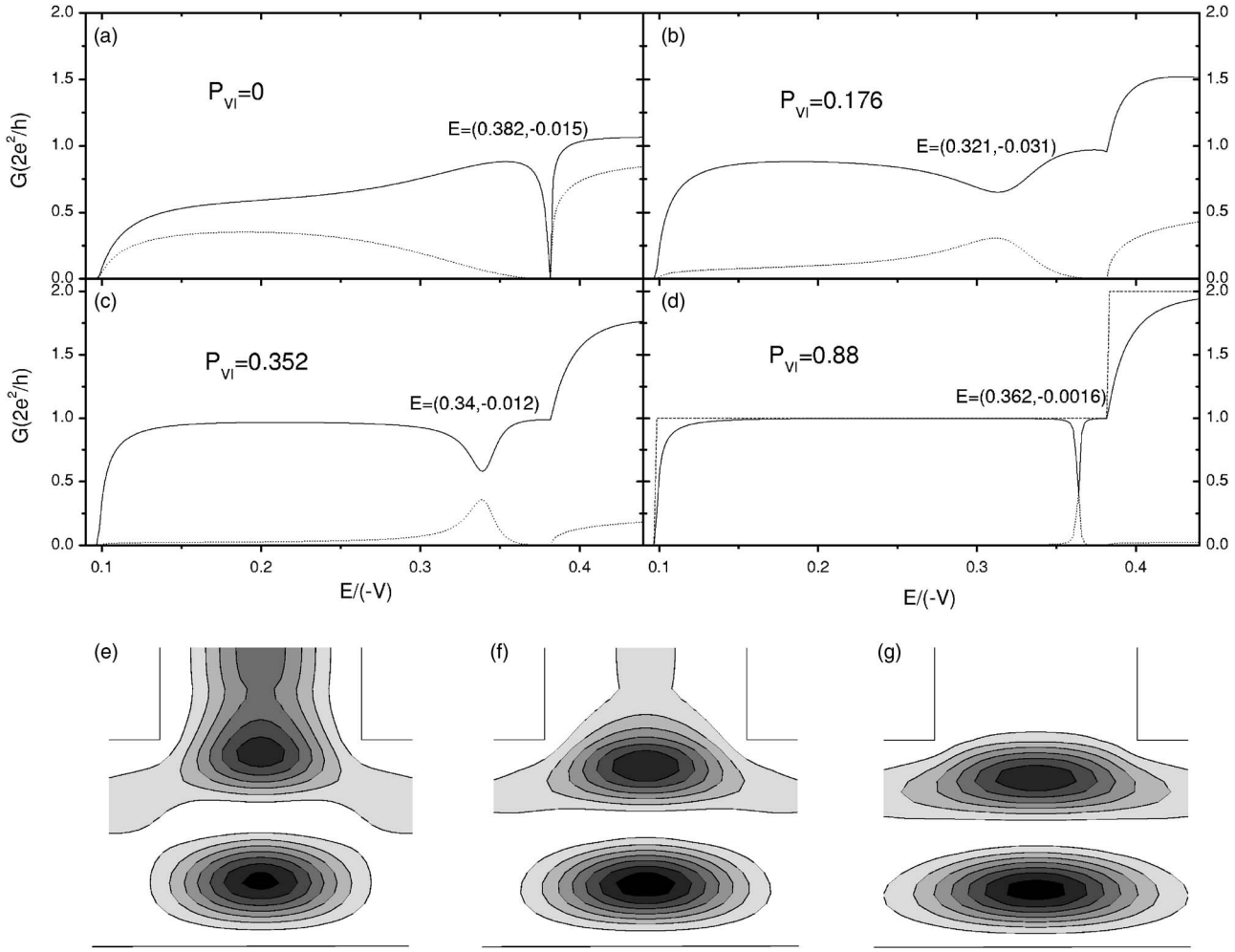

FIG. 2. (a)–(d) Conductance versus energy of electrons for a single TQWR with a different potential P_{VI} applied to region VI ($W_4 = W_1/3$). The solid and dotted lines represent the conductance straight forward $G_{\mathrm{V,I}}$ and around the bend $G_{\mathrm{VII,I}}$, respectively. (a) $P_{\mathrm{VI}}=0$, (b) $P_{\mathrm{VI}}=0.176$, (c) $P_{\mathrm{VI}}=0.352$, (d) $P_{\mathrm{VI}}=0.88$, the dashed line in (d) presents the conductance $G_{\mathrm{V,I}}$ as $P_{\mathrm{VI}}=1000$. (e)–(g) Contour plots of the probability density distributions of the quasibound state corresponding to (e) the dip peak in (b) with $E=(0.321,-0.031)$, (f) the dip peak in (c) with $E=(0.340,-0.012)$, (g) the dip peak in (d) with $E=(0.362,-0.0016)$. The more inner contour curve and darker region possesses the higher probability density.

region VI, both $G_{\mathrm{V,I}}$ and $G_{\mathrm{VII,I}}$ exist a reflection resonant dip at the energy slightly below the onset for propagation in the second mode along horizontal QWR, as shown in Fig. 2(a). The dip appears because of a resonant quasi-one-dimensional state $[E=(0.382,-0.015)]$ with a long trapping (life) time within the interaction.[4] As a potential P_{VI} is applied to region VI, however, a dip and a peak are shown in conductances straight through and around the bend, respectively [Fig. 2(b)]. The electrons with the energies around the dip peak have big probabilities of turning the corner, i.e., of entering in a horizontal lead and exiting through the vertical arm, while transmission of other electrons to vertical lead is suppressed by the potential barrier. The resonance dip-peak structure occurs as a result of coupling between incident modes and the quasibound state localized at the T junction. For the transmission around the bend, the potential barrier results in the coupling being primarily through evanescent modes, thus the resonance appears as a peak. Whereas in the horizontal direction the resonance turns out to be a dip because of the propagating mode dominating the coupling.[19] We depict in Fig. 2(e) the contour plot of the probability density $|\Psi\Psi^*|$ of the quasibound state with eigenenergy $E=(0.321,-0.031)$, the more inner contour curve and darker region possessing the higher probability density. Due to the relatively large imaginary $\gamma=0.031$ of value E representing a small lifetime τ of the quasibound state, the resonance dip-peak structure in conductance profile is wide. As the height of the potential is increased, the dip-peak couple in conductance becomes narrower and sharper and shifts to the onset of the second mode [see Figs. 2(c) and 2(d)]. The electrons transmission around the bend is further suppressed except electrons with energies near the dip peak, while transport going forward is enhanced and gradually recovers quantized phenomenon. The dip-peak structures in Figs. 2(c) and 2(d) are, respectively, induced by the quasibound states with eigenenergies $E=(0.340,-0.012)$ and $E=(0.362,-0.016)$. The quasibound state energy increases with the potential height, leading to the shifting of the dip-peak structure.

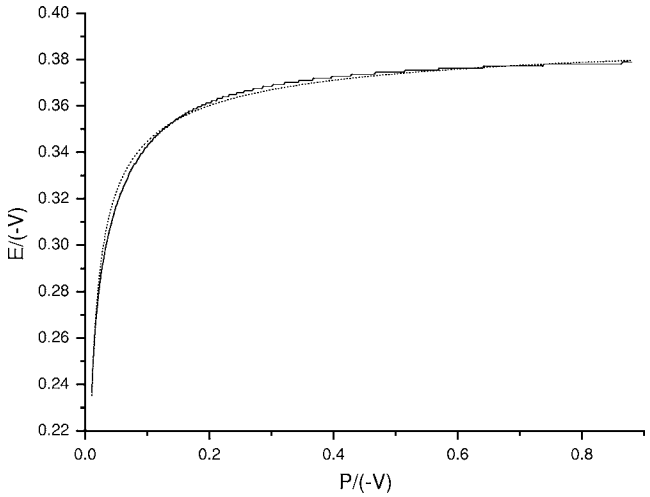

FIG. 3. Quasibound state energy E of a single TQWR as a function of the potential P_{VI} in vertical arm with $W_4=W_1/3$. The dotted line represents the curve $E=E_2'(1-(P*-V)^{-1/2})$ with $E_2'=0.389$.

While the structure being narrower and sharper results from the lifetime increase of the quasibound state. In Figs. 2(f) and 2(g), we show the contour plots of the probability density distribution of the two states. It is seen that the wave function is gradually purged out of the vertical arm by a higher potential barrier and extended to the parallel QWR. As expected, the conductance straight forward is a completely formed quantization plateau [see dashed line in Fig. 2(d)], as the potential modulation is strong enough. In this case, the wave function is completely purged out of the vertical arm and the coupling of the vertical arm and the parallel QWR vanishes. To more clearly show the dependence of the quasibound state on the potential barrier, we depict in Fig. 3 the quasibound state energy as a function of the potential height P_{VI}. One can see from the figure that the quasibound state energy behaves like a cure of $E=E_2'[1-(P*-V)^{-1/2}]$ [the dotted line], where E_2' is slightly greater than the threshold energy of the second mode. It rapidly increases with the potential height at lower potential, and slowly approaches the threshold of the second mode with higher potential.

In Figs. 4(a) and 4(b), the conductance for a single TQWR in Fig. 1(a) with different thickness W_4 of potential barrier VI are calculated. Comparing Fig. 4(a) with Fig. 2(b), the dip-peak couple structure in conductance becomes more pronounced and shifts toward the lower energy, as W_4 is increased from $W_1/3$ to W_1. It is originated from the fact that

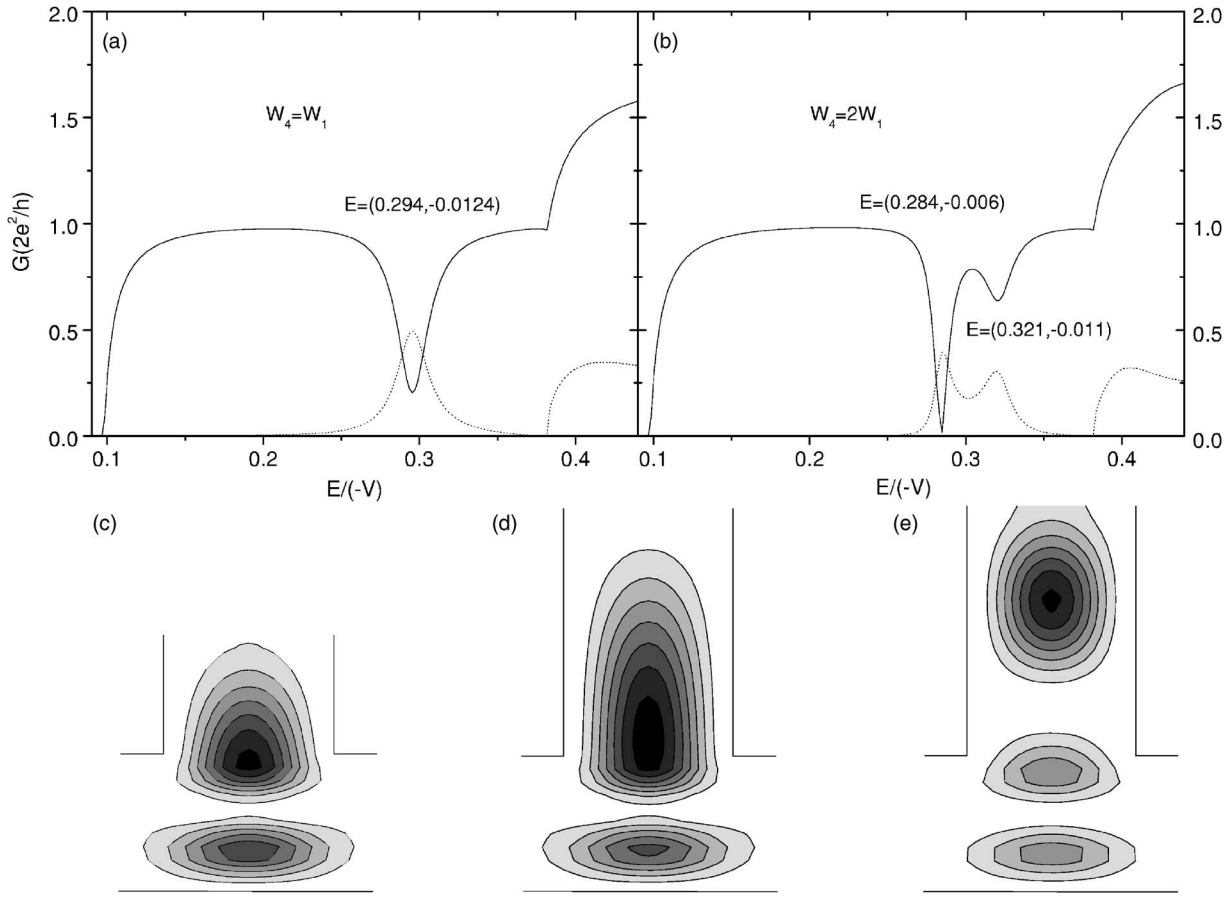

FIG. 4. (a) and (b) Conductance versus electron energy for a single TQWR with different potential thickness W_4 ($P_{\mathrm{VI}}=0.176$); (a) $W_4=W_1$, (b) $W_4=2W_1$. The solid and dotted lines represent the conductance going forward $G_{\mathrm{V,I}}$ and around the bend $G_{\mathrm{VII,I}}$, respectively. (c)–(e) Contour plots of the probability density distribution of the quasibound states corresponding to (c) the dip peak in (a) with $E=(0.294, -0.0124)$, (d) the first dip peak in (b) with $E=(0.284,-0.006)$, (e) the second dip peak in (b) with $E=(0.321,-0.011)$. The more inner contour curve and darker region possesses the higher probability density.

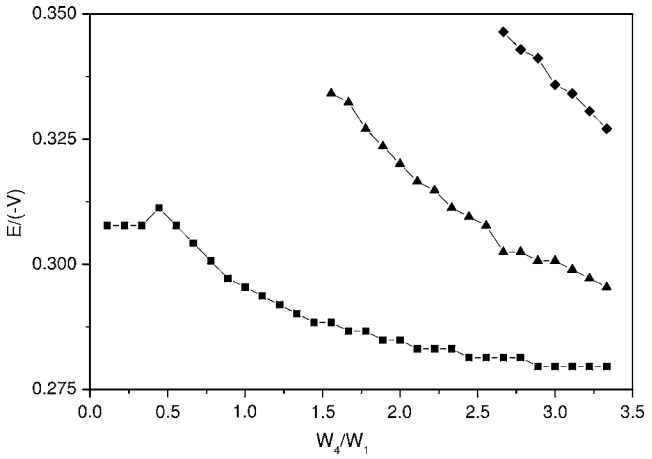

FIG. 5. Quasibound state energy of a single TQWR as a function of the potential thickness W_4 with $P_{VI}=0.176$, the solid square, solid up triangle, and solid rhombus represent the first, second, and third quasibound state energies, respectively.

the variation of the potential thickness gives rise to the eigenenergy of the quasibound state moving from $E=(0.320,-0.031)$ to $E=(0.294,-0.0124)$. The contour plot of the probability density distribution of the state, as shown in Fig. 4(c), also exhibits the electrons having bigger probabilities of staying at the junction with thicker potential barrier. As the thickness is further increased to $2W_1$, two couples of dip peak induced by the quasibound states are shown in the conductance profile, the first dip nearly turning into a transmission zero [Fig. 4(b)]. It indicates that there are two quasibound states existing in the T junction. In Figs. 4(d) and 4(e), we plot the contour of the probability density of the two quasibound states, respectively, with energies $E=(0.284,-0.006)$ and $E=(0.321,-0.011)$. The thickness increase leads to the wave function of the quasibound states localized deeply into the vertical arm. In addition, it is also found from Figs. 4(a) and 4(b) that the conductance of low-energy electrons is nearly unchanged with the variation of W_4. This case is somewhat like the case caused by length variation of T stub in Ref. 11. It can be interpreted that electrons with a relatively low energy cannot penetrate through the barrier thus are insensitive to changes of potential thickness. In Fig. 5, we display the relation of quasibound states and the potential thickness. Two features deserve special attention. One is the quasibound state energies decrease with the thickness increase. The other is, as W_4 is added to $(n+0.5)W_1$, another

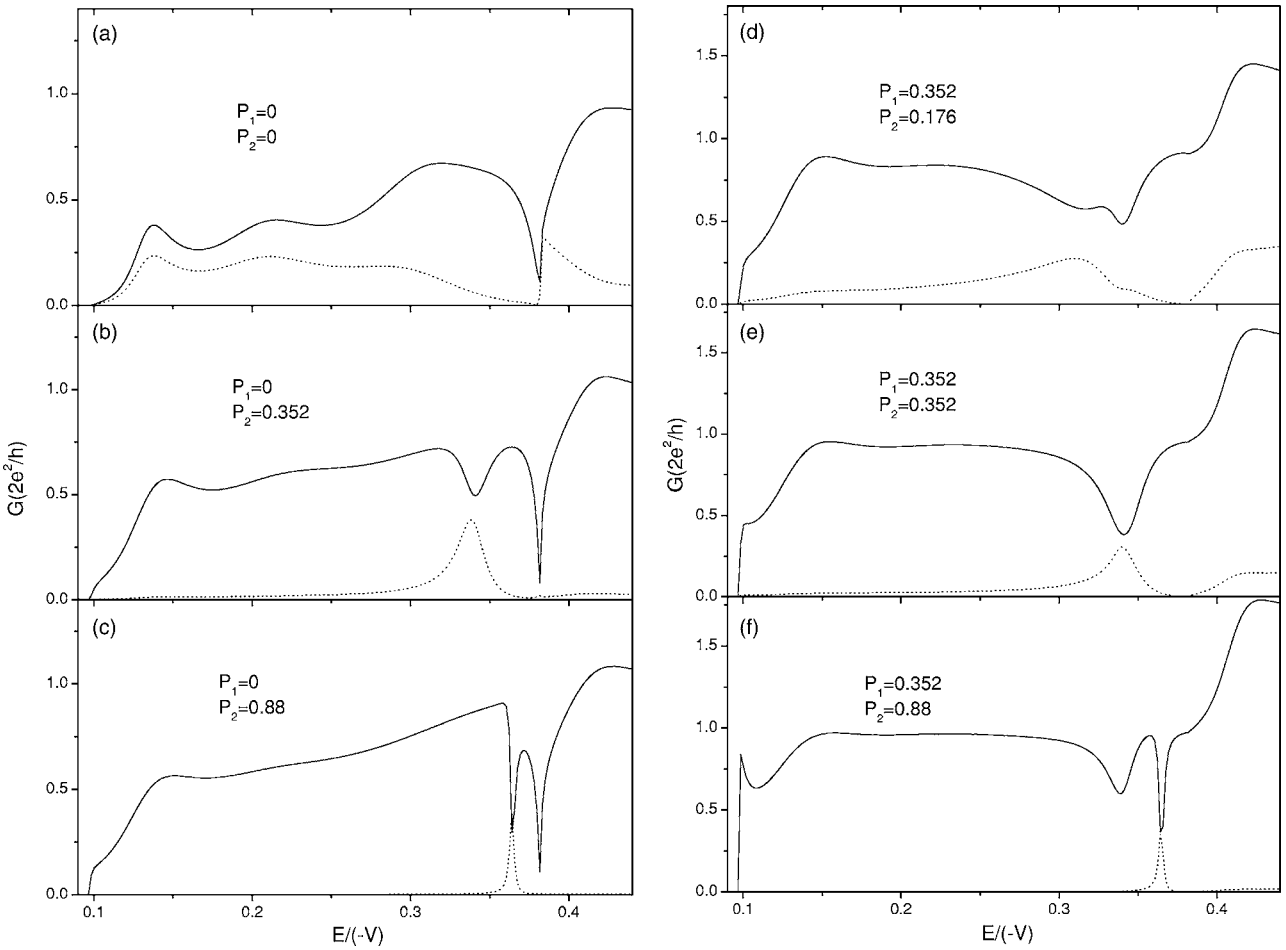

FIG. 6. Conductance for two coupled TQWR with a different potential P_1, P_2, respectively, applied to region 1, 2 ($W_5=W_6=W_1/3$), (a) $P_1=0$, $P_2=0$, (b) $P_1=0$, $P_2=0.352$, (c) $P_1=0$, $P_2=0.88$, (d) $P_1=0.352$, $P_2=0.176$, (e) $P_1=0.352$, $P_2=0.352$, (f) $P_1=0.352$, $P_2=0.88$. The solid and dotted lines, respectively, represent the conductance straight through $G_{V,I}$ and around the second bend $G_{VII,I}$ (from lead I to lead VII).

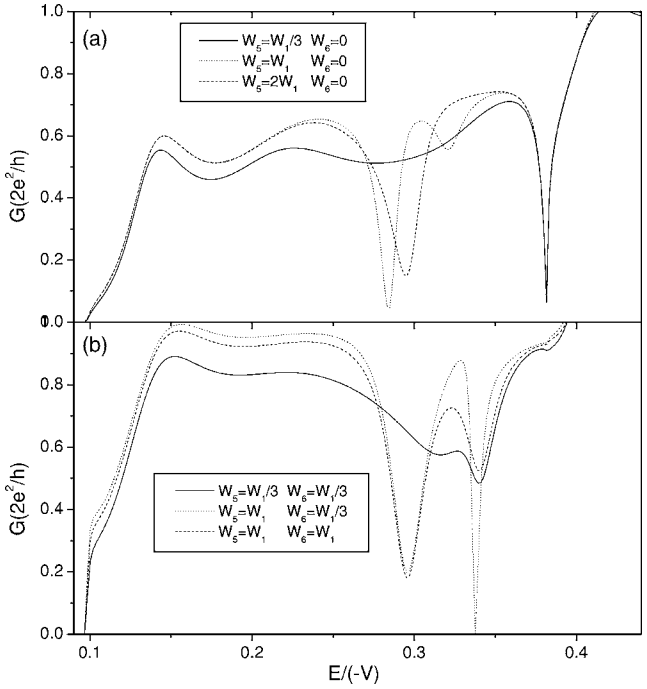

FIG. 7. Conductance going forward $G_{V,I}$ versus electron energy for two coupled TQWR: with different potential thickness as W_5 and W_6, as the potentials P_1 and P_2 applied to regions 1 and 2, respectively. (a) $P_1=0.176$ and $P_2=0$, $W_5=W_1/3$ for solid line, $W_5=W_1$ for dashed line and $W_5=2W_1$ for dotted line. (b) $P_1=0.176$ and $P_2=0.352$, $W_5=W_6=W_1/3$ for solid line, $W_5=3W_6=W_1$ for dashed line, and $W_5=W_6=W_1$ for dotted line.

quasibound state will appear in the high energy region of the first mode. From these results, we can conclude that the transport properties of TQWR are sensitive to the potential modulation in vertical arm.

By cascading two single TQWR, separated by a region of length W_4, we obtain the configuration of two coupled TQWR, where two vertical leads VI and VII are connected to horizontal QWR by regions 1 and 2, respectively [see Fig. 1(b)]. It is known that transport properties of the coupled TQWR are dependent on the length W_4,[4] due to quantum interference in the scattering from the two T junctions. Here, we concentrate on the effect of potential modulation on electron transport, fixing $W_1=W_2=W_3=W_4$. The calculated conductance for the coupled TQWR as a function of electron energy are depicted in Fig. 6. Figures 6(a)–6(c) display the conductance for case of only P_2 is applied to region 2 of the coupled TQWR, and Figs. 6(d)–6(f) display the conductance for case of both P_1 and P_2 are applied to regions 1 and 2 respectively. Comparing with the isolated wire case, the coupled wire case shows sharper modulation and more oscillations in conductance profile, which is ascribed to the coherence between left and right TQWR. The comparison also shows that the conductance straight through and around the bend keep the feature of those in a single TQWR case. The increase of potential weakens the transmission around the corner while strengthens the transport of electrons going forward. In particular, each potential barrier in the vertical arm induces a dip-peak couple structure which shifts to high energy and becomes narrow and sharp with the potential modulation. Each dip-peak couple corresponds to a quasibound state localized at the T junction. In Fig. 7, we show the conductance straight through the coupled TQWR with different potential thicknesses W_5 and W_6 of regions 1 and 2. It is clear that the thickness has obvious modulation on the oscillations of conductance, due to the influence of the thickness on the quasibound states localized at the junctions, especially the high-energy region of the first mode. For the case where only a potential P_1 is applied to region 1, we compare in Fig. 7(a) conductance for three different thickness W_5 of the barrier: $W_1/3$, W_1, and $2W_1$. As in the single QW case, the thicker the potential barrier, the more prominent the conductance oscillations. The first dip drops with the increase of the potential thickness W_5, dividing the plateau of the first mode into two parts. For the case where two potentials P_1 and P_2 are applied to regions 1 and 2, respectively ($P_1<P_2$), we compare conductance with different potential thickness W_5 and W_6. In the case of thin barriers ($W_5=W_6=W_1/3$) [see solid line in Fig. 7(b) or Fig. 6(d)], two shallow dips induced by modulation of P_1 and P_2 appear, respectively, at $E\approx 0.315$ and $E\approx 0.339$. The individual increase of the thickness of regions 1 and 2 sharpens their corresponding dips, as shown by dashed and dotted lines in Fig. 7(b), and oscillation around the two dips becomes very drastic. These results demonstrate that conductance profiles of TQWR can be tailored by the potential modulation in the vertical arm, thus different conductance profiles are obtained, as the modulation of QWR width on TQWR.[5]

IV. CONCLUSIONS

We have developed a LGF method suited to calculate the electronic transport properties of multiterminal nanostructures. Using the method, the influence of the potential barrier in vertical arms on electronic transport across one or two coupled TQWR is studied. It is shown that, for a TQWR, the potential barrier changes the energy of the quasibound state localized at the T junction. While each quasibound state induces a dip-peak couple structure in the conductance straight through and around the bend. The modulation of the potential thickness leads to the dip-peak couple being more pronounced, and the number of the dip-peak couple is closely related to the potential thickness. For two coupled TQWR, the two dips in conductance going forward are closely correlated to the potential barriers. Various conductance profiles can be obtained by the potential modulation on coupled TQWR.

ACKNOWLEDGMENTS

This work was supported by the Major Project of State Ministry of China (Grant No. 204099) and the Project Supported by Scientific Research Fund of Hunan Provincial Education Department (No. 02C572).

*Corresponding author; email address: xhyan@xtu.edu.cn

[1] Yia-Chung Chang, L. L. Chang, and L. Esaki, Appl. Phys. Lett. **47**, 1324 (1985).

[2] Loren Pfeiffer, K. W. West, H. L. Stormer, J. P. Eisenstein, K. W. Baldwin, D. Gershoni, and J. Spector, Appl. Phys. Lett. **56**, 1697 (1990); A. R. Goñi, L. N. Pfeiffer, K. W. West, A. Pinczuk, H. U. Baranger, and H. L. Stormer, *ibid.* **61**, 1956 (1992).

[3] M. H. Szymanska, P. B. Littlewood, and R. J. Needs, Phys. Rev. B **63**, 205317 (2001); M. Stopa, *ibid.* **63**, 195312 (2001); H. Akiyama, T. Someya, and H. Sakaki, *ibid.* **53**, R16160 (1996).

[4] Harold U. Baranger, Phys. Rev. B **42**, 11479 (1990).

[5] G. Goldoni, F. Rossi, and E. Molinari, Appl. Phys. Lett. **71**, 1519 (1997).

[6] J. L. Bohn, Phys. Rev. B **56**, 4132 (1997).

[7] M. Grundmann, O. Stier, A. Schliwa, and D. Bimberg, Phys. Rev. B **61**, 1744 (2000).

[8] Y. K. Lin, Y. N. Chen, and D. S. Chuu, Phys. Rev. B **64**, 193316 (2001); J. Appl. Phys. **91**, 3054 (2002).

[9] L. A. Openov, Europhys. Lett. **55**, 539 (2001).

[10] Toshihiro Itoh, Phys. Rev. B **52**, 1508 (1995).

[11] Fernando Sols, M. Macucci, U. Ravaioli, and Karl Hess, Appl. Phys. Lett. **54**, 350 (1989); J. Appl. Phys. **66**, 3892 (1989).

[12] T. Ando, Phys. Rev. B **44**, 8017 (1991).

[13] D. Guan, U. Ravaioli, R. W. Giannetta, M. Hannan, I. Adesida, and M. R. Melloch, Phys. Rev. B **67**, 205328 (2003).

[14] Supriyo Datta, *Electronic Transport in Mesoscopic Systems* (Cambridge University Press, Cambridge, England, 1997).

[15] Michael J. McLennan, Yong Lee, and Supriyo Datta, Phys. Rev. B **43**, 13846 (1991).

[16] H. Q. Xu, Phys. Rev. B **66**, 165305 (2002).

[17] T. C. L. G. Sollner, E. R. Brown, W. D. Goodhue, and H. Q. Le, Appl. Phys. Lett. **50**, 332 (1987); Zhi-an Shao, Wolfgang Porod, and Craig S. Lent, Phys. Rev. B **49**, 7453 (1994).

[18] A. Weisshaar, J. Lary, S. M. Goodnick, and V. K. Tripathi, Appl. Phys. Lett. **55**, 2114 (1989).

[19] P. J. Price, Phys. Rev. B **48**, 17301 (1993); Semicond. Sci. Technol. **9**, 899 (1994).